Supplementary Information for

An ensemble of interconverting conformations of the elemental paused transcription complex creates regulatory options

Jin Young Kang[a,1], Tatiana V. Mishanina[b,1], Yu Bao[c,1], James Chen[d], Eliza Llewellyn[d], James Liu[c], Seth A. Darst[c,2], Robert Landick[c,e,2]

Author affiliations: [a]Department of Chemistry, Korea Advanced Institute of Science and Technology, Daejon 34141, Republic of Korea; [b]Department of Chemistry and Biochemistry, University of California San Diego, La Jolla, CA 92093, United States; [c]Department of Biochemistry, University of Wisconsin-Madison, Madison, WI 53706, United States; [d]Laboratory of Molecular Biophysics, The Rockefeller University, New York, NY 10065, United States; [e]Department of Bacteriology, University of Wisconsin-Madison, Madison, WI 53706, United States.

This PDF file includes:

1. Expanded Materials and Methods
2. Abbreviations Used in Main Text and Supplement
3. SI Tables
    - Table S1. E. coli RNAP structural modules.
    - Table S2. Oligonucleotides and plasmids used in this study.
    - Table S3. Cryo-EM data acquisition and refinement parameters.
    - Table S4. EC and PEC structures, states, and conformational features.
    - Table S5. Half-map analysis of swivel angles.
4. SI Figures
    - Figure S1. *con*-ePECs rapidly equilibrate between various translocation states following nucleotide addition.
    - Figure S2. Cryo-EM processing for *con*-ePEC-1 and *con*-ePEC.
    - Figure S3: The upstream fork junction of pre-translocated *con*-ePEC rearranges when the TL unfolds.
    - Figure S4. Cryo-EM processing for *his*-ePEC.
    - Figure S5. Cys-triplet reporter analysis of ePEC conformations.
    - Figure S6. Nun-locked catalysis assay of ePEC translocation register.
    - Figure S7. Conformational changes in EC conversion to con-ePEC.
    - Figure S8.Conformational states of the *his*-ePEC.
    - Figure S9. Rate constants used for modeling distributions of ePEC states.
5. SI References

Expanded Materials and Methods

Eco RNAP expression and purification

Δα-CTD *Eco*RNAP for cryo-EM experiments was prepared largely as described previously (1, 2). Briefly, a pET-based plasmid that contains *rpoA* (α) that contains PreScission cleavage site between N-terminal and C-terminal domains and a deca-histidine tag at the C-terminus, *rpoB* (β), *rpoC* (β′) and *rpoZ* (ω) was co-expressed with a pACYCDuet-1 plasmid contained *rpoZ* in BL21(DE3) (Novagen). The cells were grown at 37 ºC in LB broth media in the presence of 100 ug ampicillin/mL and 34 ug chloramphenicol/mL, and transferred to 30 ºC when apparent OD_{600} reached 0.3. Protein expression was induced at apparent OD_{600} of 0.6-0.8 by addition of isopropyl β-D-thiogalactopyranoside (IPTG) to a final concentration of 1 mM, then further growth for 4 h. Cells were harvested, resuspended in lysis buffer [50 mM Tris pH 8.0, 5% glycerol, 1 mM EDTA (pH 8.0), 1 mM $ZnCl_2$, 10 mM DTT, protease inhibitor cocktail], and lysed by French Press (Avestin) at 4 ºC. The lysate was centrifuged at 14000 rpm, 4°C for 30 minutes twice, and the supernatant was precipitated by adding polyethyleneimine [PEI, 10% (w/v), Sigma Aldrich] to a final concentration of 0.6% (w/v) dropwise. The pellets were washed three times with wash buffer containing TGED (10 mM Tris pH 8.0, 5% glycerol, 0.1% EDTA pH 8.0, 10 mM DTT) + 0.5M NaCl, and the RNAP was eluted from the pellet with elution buffer (TGED + 1 M NaCl). The eluted RNAP was precipitated by adding ammonium sulfate (35 g per 100 ml eluted protein solution), redissolved in chelating buffer (20 mM Tris pH 8.0, 1 M NaCl, 5% glycerol), and loaded onto Hitrap IMAC HP columns (Cytiva) for purification by Ni^{2+}-affinity chromatography using an imidazole gradient. The recovered RNAP was dialyzed overnight into TGED + 100 mM NaCl buffer in the presence of PreScission protease to remove C-terminal domain of α subunit (α-CTD) and deca-histidine tag. The dialyzed protein was passed through Hitrap IMAC HP column to remove uncleaved protein, and loaded onto a Biorex-70 column (Bio-rad) for ion exchange chromatography using an NaCl gradient. The eluted RNAP by was concentrated by Amicon Ultra centrifugal filter (Merck Millipore), and loaded onto a HiLoad 26/600 Superdex 200 pg column (Cytiva) equilibrated with SEC buffer (TGED + 0.5 M NaCl) for size-exclusion chromatography. The purified protein was supplemented with glycerol to 15%, flash-frozen in liquid nitrogen, and stored at –80 ºC until use.

*Eco*RNAP for biochemical assays was prepared as described previously (3).

EC preparation for cryo-EM

Synthetic DNA and RNA oligonucleotides were obtained from Integrated DNA Technologies (Coralville, IA) (Table S2). The RNA was gel-purified before use. The nucleic acids were dissolved in RNase-free water (Ambion/ThermoFisher Scientific, Waltham, MA) to 0.2–1 mM. Template DNA and RNA were annealed at a 1:1 ratio in a thermocycler (95 °C for 2 min, 75 °C for 2 min, 45 °C for 5 min, followed by a steady cooling to 25 °C at 1°C/min). The annealed RNA-DNA hybrid was stored at –80 °C until use. Purified *Eco* RNAP was buffer-exchanged using a Superose 6 INCREASE (Cytiva) column into cryo-EM buffer (20 mM Tris-HCl, pH 8.0, 150 mM potassium glutamate, 5 mM $MgCl_2$, 5 mM DTT). The eluted protein was mixed with the pre-formed RNA-DNA hybrid at a molar ratio of 1:1.3 and incubated for 15 min at room temperature. Additional $MgCl_2$ (final 5 mM) and non-template DNA (final 1.3 ratio relative to RNAP) were added and incubated for 10 min at room temperature to complete EC formation. The complexes were concentrated by centrifugal filtration in an Amicon unit (MWCO 100k, EMD Millipore, Billerica, MA) to 4.0-5.5 mg RNAP/mL before grid preparation.

Cryo-EM grid preparation

Before freezing, CHAPSO was added to an 8 mM final concentration to the samples (4). C-flat (Protochips, Morrisville, NC) CF-1.2/1.3 400 mesh gold grids or Quantifoil R 1.2/1.3 Cu 400 grids were glow-charged for 15 s prior to the application of 3.5 µl of the EC sample. For *con*-ePEC$_{-1}$ and *his*-ePEC, the samples were directly applied to the grid. For *con*-ePEC, the assembled ePEC$_{-1}$ was mixed with 1 mM rCTP by pipetting and applied to the cryo-EM grid (total time from rCTP addition to freezing was ~14 s). The grids were blotted and plunge-frozen in liquid ethane using a Vitrobot mark IV (FEI, Hillsboro, OR) with 100% chamber humidity at 23°C.

Cryo-EM data acquisition and processing

Structural biology software was accessed through the SBGrid consortium (5).

All grids were imaged using a 300 keV Titan Krios (ThermoFisher Scientific) equipped with a K2 Summit direct electron detector (Gatan, Pleasanton, CA). Images were recorded with SerialEM (6) in super-resolution mode with a super-resolution pixel size of 0.650 Å and a defocus range of –0.8 to –2.4 μm. Data were collected with a dose rate of 8 electrons/physical pixel/s (1.3 Å pixel size at the specimen). Images were recorded with a 10 s exposure and 0.2 s sub-frames (50 total frames) with a dose rate of 8 electrons/physical pixel/s (1.3 Å pixel size at the specimen) to give a total dose of 47.34 electrons/Å^2. Dose fractionated subframes were 2 x 2 binned (giving a pixel size of 1.3 Å), aligned and summed using MotionCor2 (7). The contrast transfer function was estimated for each summed image using Gctf (8). Data were further processed using RELION (9) or CryoSPARC2 (CS2) (10), as described below. The local resolution estimation and filtration of all the final maps were done by the blocres and blocfilt commands in the bsoft (11).

***con*-ePEC$_{-1}$.** Particles were automatically picked in Gautomatch (http://www.mrc-lmb.cam.ac.uk/kzhang/) using templates and the picked particles were subjected to 3D consensus refinement in RELION (9). The focused classification was performed on the SI3 domain with subtracted particles and one class among four classes was pulled, reverted, and 3D refined. The particles were subjected to another 3D classification into three classes, and the best class having 213,041 particles was CTF refined and particle polished iteratively until the map was not improved anymore. The final map was sharpened by postprocessing.

***con*-ePEC**. Particles were picked using template picker in CS2 and subjected to heterogenous refinement with two sets of three templates generated from CS2 Ab-initio reconstruction. Among the six classes, two classes were pulled and subjected to another run of heterogenous refinement using three sets of the two templates from the previous heterogenous refinement. Among the classes, two classes were selected, homogeneous refined, and transferred to RELION for further CTF refinement and particle polishing. Each class was iteratively 3D refined after particle polishing and CTF refinement until the class was not improved further. The two maps – *con*-ePEC_fTL (162.8k particles) and *con*-ePEC_ufTL (197.9k particles) – were sharpened by postprocessing.

***his*-ePEC.** Particles were picked by Gautomatch and subjected to 2D classification in CS2. The extracted particles were classified in heterogenous refinement into 3 classes, and the best class

having 880,989 particles were homogeneous refined and transferred to RELION for further processing. The transferred particles were 3D classified into three classes and 3D auto-refined. Then each map was CTF refined, particle-polished, and again 3D auto-refined. Among the three classes, one class having 432.3k particles achieved 3.3 Å resolution (*his*-ePEC_ufTL1) and the other class having 210.6k particles achieved 5.6 Å resolution (*his*-ePEC_ufTL2). The third class, which contained a folded-TL (fTL), was further subjected to focused classification (focusing on the RH-FL) into three classes. The three classes were reverted and 3D auto-refined yielding *his*-ePEC_fTL-Fin2 (29.6k particles), *his*-ePEC_fTL-Fin1 (150.9k particles), and *his*-ePEC_fTL-Fout (57.5 k particles) maps.

Model building, refinement and validation

To build initial models, Eco EC (PDB 6C6T) (12) was fitted into the electron density maps using Chimera (13). These initial models were real-space refined against the post-processed map using Phenix (14). In the refinement, domains in the core and nucleic acids were rigid-body refined, then subsequently refined with secondary structure restraints.

Swivel angle determinations

6RH3 was used as the reference structure (swivel angle = 0°).(15) To determine the swivel angle for a test Eco RNAP structure, the test structure was superimposed with 6RH3 via a-carbon atoms of the structural Core module (Table S1) using the following PyMOL command:

> align (test and (chain G or chain H or (chain I and (res 3:27 or res 142:152 or res 445:455 or res 520:713 or res 786:828 or res 1060:1240)) or (chain J and (res 343:368 or res 421:636)) or chain K) and name CA),(6RH3 and (chain G or chain H or (chain I and (res 3:27 or res 142:152 or res 445:455 or res 520:713 or res 786:828 or res 1060:1240)) or (chain J and (res 343:368 or res 421:636)) or chain K) and name CA)

Objects comprising the swivel modules from each structure were then generated using the following PyMOL commands:

> create 6rh3_swivel,(6rh3 and ((chain C and res 1241:1341) or (chain D and (res 1:342 or res 369:420 or res 787:930 or res 1135:1375))))

> create test_swivel,(6rh3 and ((chain I and res 1241:1341) or (chain J and (res 1:342 or res 369:420 or res 787:930 or res 1135:1375))))

The rotation axis and rotation angle transforming one swivel module into the other was then computed using the PyMOL script draw_rotation_axis_v2.py (http://pymolwiki.org/index.php/RotationAxis):

```
run draw_rotation_axis_v2
draw_axis('test_swivel','6rh3_swivel')
```

To assess the significance and reproducibility of the swivel angle determinations, we performed swivel-angle analyses using so-called half-maps (calculated normally in the cryo-EM pipeline to calculate FSC curves). For the structures with swivel angle = (0°), we assess that the swivel angle is < ~0.5° and that the rotation angle/axis determination algorithm cannot determine the rotation angle/axis reliably. For rotation angle >~0.5°, the rotation axis was consistently determined. We used rigid-body refinements for this assessment. In our experience, full-atom refinement yields insignificant changes estimate in the swivel angle determination (< 0.2°). We used two different starting models (to make sure the results didn't depend dramatically on the swivel angle of the starting model), one was a model based on 6RH3 (swivel angle = 0°, swivel0), the other was a model based on the largest swivel angle in our data (his-ePEC_ufTL1, swivel angle = 3.8°, swivel3.8). For each half-map, we performed two rigid-body refinements (one starting with swivel0 and one starting with swivel3.8). We then calculated the swivel angle as described above. This analysis generated four independent swivel angles for each structure (swivel0 refined against half-map1, swivel0 refined against half-map2, swivel3.8 refined against half-map1, swivel3.8 refined against half-map2), allowing the calculation of an average half-map swivel angle and standard deviation (Table S5). These values, within error, match the original swivel angles calculated from the full maps, and the same trends were maintained. The error in the small swivel angles (~0.5 << angle < ~1.5°) is around 30%, whereas the larger swivel angles yielded errors less than 10%. This analysis established that the swivel-angle determination is robust and reproducible.

In vitro transcription pause assays with wild-type or Cys-pair reporter RNAPs

The CPR protein was prepared as described previously (3). The transcription assay scaffold was made by mixing 5 μM RNA with 10 μM template strand DNA (t-DNA) in Reconstitution Buffer (10 mM Tris-HCl, pH 7.9, 5 mM $MgCl_2$, 40 mM KCl) or cryo-EM buffer (20 mM Tris-Cl, pH 8.0, 150 mM potassium glutamate, 5 mM $MgCl_2$, 5 mM DTT) followed by heat-denaturing and gradual cooling in thermal cycler. Elongation complex (EC) was formed by mixing scaffold with CPR or ΔαCTD RNAP at 1: 3 ratio in Elongation Buffer (25 mM HEPES-KOH, pH 8.0, 130 mM KCl, 5 mM $MgCl_2$, 0.15 mM EDTA, 5% v/v glycerol, 25 μg acetylated BSA/mL) or cryo-EM buffer above for 15 min at 37 °C or 23 ºC (Fig. S1) followed by adding non-template strand DNA (nt-DNA) for 15 min (1 μM RNA, 2 μM T-DNA, 3 μM RNAP, 5 μM NT-DNA). CHAPSO was added to a final concentration of 8 mM to ECs reconstituted in cryo-EM buffer. Free RNAP was blocked by adding 0.1 mg heparin/mL. To induce disulfide bond formation, 5 mM H_2O_2 was added for 15 min at 37 °C followed by adding 0.1 U/μL catalase for 5 min at room temperature to remove access H_2O_2.

For *con*-ePEC pause assay with varying delay times of GTP addition (Fig. S2), G16 RNA was 5'-^{32}P labeled prior to scaffold annealing. Following *con*-ePEC$_{-1}$ assembly at 23 ºC (mimicking cryo-EM sample preparation conditions), complexes were diluted to a final concentration of 50 nM based on RNA with cryo-EM buffer and reacted with CTP (100 μM final) for the indicated amount of time at 23 ºC, to position RNAP at the pause (Fig. S2). Escape from the pause was then initiated by addition of limiting GTP (10 μM) at 23 ºC and followed by withdrawing aliquots at various time points (see plot in Fig. S1C for specific time points).

For *con*-ePEC pause assay using CPR RNAP, reconstituted EC was adjusted to 200 nM with EB and isotope-labeled with [α-^{32}P] GTP (33 Ci/mmol) to reach G16 pause –1 register. Transcription was initiated by adding equal volume of GTP and CTP mixture (100 μM final) and incubated at 37 °C. 5 μL of reaction samples were taken at different time points over 2 min and mixed with 5 μL of Stop Buffer (8 M urea, 50 mM EDTA, 90 mM Tris-borate buffer, pH 8.3, 0.02% bromophenol blue, 0.02% xylene cyanol) to quench the reaction. RNAs were analyzed by denaturing PAGE (15% 19:1 acrylamide: bis-acrylamide, 45 mM Tris-borate, pH=8.3, 1.25 mM

Na_2EDTA, 8 M urea). For *his*-ePEC/*his*PEC pause assay, reconstituted EC was adjusted to 200 nM with EB, isotope-labeled with [α-^{32}P]CTP (33 Ci/mmol), and extended to U20 pause register with 2 μM UTP. To mimic pause RNA hairpin, 2 μM antisense RNA oligo was added for 10 min at 37 °C. Transcription was initiated by adding equal volume of GTP mixture (10 μM final) and incubating at 37 °C. For non-CPR transcription assays, CPR was replaced by WT RNAP and crosslinking steps were omitted.

Cys-triplet reporter (CTR) crosslinking assay

The CTR RNAP was prepared as described previously (3). The CTR EC was reconstituted similarly to the transcription assay with a few adjustments in component ratio (5 μM RNA, 10 μM t-DNA, 2.5 μM CTR, 10 μM nt-DNA). To induce disulfide bond formation, 5 mM H_2O_2 was added for 15 min at 37 °C followed by adding 0.1 U catalase/μL for 5 min at room temperature to remove access H_2O_2. NTPs (50 μM each) were used for extension to relevant EC/PEC registers and 25 μM antisense RNA oligo was used to mimic pause RNA hairpin. Samples were mixed with 4× LDS Sample Buffer (ThermoFisher) and analyzed on a thin layer 4-15% gradient polyacrylamide gel (GE Healthcare) using a PhastSystem Electrophoresis Unit (Pharmacia). The intensities of β–β′ and β′–β′ species were gel-quantified and used for SPB calculation: SPB = (β′–β′%) / (β–β′%).

Translocation register assay

EC scaffolds were prepared as described above with 5′ end ^{32}P isotope labeled RNAs. The ECs were reconstituted by mixing scaffold with β′-His10 tagged WT RNAP at 1:1 ratio in cryo-EM PEC Buffer (20 mM Tris-HCl, pH=8.0, 150 mM potassium glutamate, 5 mM $MgCl_2$) for 15 min at 25 °C followed by adding non-template strand DNA (NT-DNA) for 10 min (2 μM RNA, 4 μM T-DNA, 2 μM RNAP, 10 μM NT-DNA). Both *con*-ePEC and *his*-ePEC were directly reconstituted at –1 pause register. Reconstituted ECs were adjusted to 200 nM with buffer and incubated with 8 mM CHAPSO (to mimic cryo-EM sample preparation condition) and 0.1 mg/mL heparin. ECs were immobilized on Ni^{2+} NTA magnetic beads (Dynabeads, ThermoFisher) and incubated with 200 μM CTP or UTP for 1 min to make con-ePEC and *his*-

ePEC respectively. To form *his*PEC, 2 μM antisense RNA oligo was added to *his*-ePEC for 5 min. To trap translocation states of PECs, 15 μM coliphage HK022 Nun protein (Kang et al., 2017) was added for 5 min incubation. Supernatant was then removed and bead-tethered PECs were washed with buffer twice. To elute PECs, incubate beads with cryo-EM PEC buffer containing 150 μM imidazole for 10 min at 25 °C. PECs were incubated with either 2.5 μM pyrophosphate for 5 min to test pyrophosphorolysis efficiency or 1 mM NTPs for 2 min to test nucleotide addition efficiency. Samples were mixed with equal volume of Stop buffer for PAGE analysis.

Kinetic and thermodynamic modeling of multiple state elemental pausing

The relative particle distributions for *con*-ePEC and *his*-ePEC were used to fit kinetic models with fixed forward rates of 100 s^{-1} (right to left in Fig. 7A) and floating reverse rates over a 10 s window. We note that, for parsimony, our modeling that assumes all cryo-EM–detected states are paused. It is possible that small amounts of active ECs are intermixed with some states because they are structurally indistinguishable at currently achievable cryo-EM resolutions. These models were fit using Kintek Explorer (16) to constant levels of pause intermediates A–F corresponding to the cryo-EM particle distributions and omitting states for which no particles were observed. Fits converged rapidly to match the observed distributions with reverse rates for *con*-ePEC of (D-to-B) 122 s^{-1} and for *his*-ePEC of (B-to-A) 18 s^{-1}, (C-to-B) 258 s^{-1}, (E-to-C) 27.5 s^{-1}, and (F-to-E) 49 s^{-1} (Fig. S9A). Using these rates and a starting population of 100% state A or B to model ePEC formation, the distributions of states A–F reached equilibrium in ~0.5 s compared to the ~14 s used to form *con*-ePECs for cryo-EM. The same overall results could be obtained (with much faster equilibration) by multiplying all of the forward and reverse rates by a factor of 10. This 10-fold increase in rates would lower $\Delta G^{\ddagger}$ without changing the relative G^0s of states A–F.

To obtain a model that included states A–F and could fit an arbitrary biphasic pausing dataset, we first generated model biphasic pause data using a two-exponential rate equation with 0.33 bypass EC (67% efficient pausing), 0.33 ePEC escaping at 0.15 s^{-1}, and 0.33 ePEC escaping at 0.03 s^{-1} (Fig. 7C; open circles). These data approximate those we observed for *his*-ePEC at 10 μM GTP (Fig. 1E) but are idealized using the two-exponential equation to provide more uniform

data for fitting the kinetic model. We included state D with initial rates that would yield less than 1% state D at equilibrium and minor adjustments to other reverse rates (relative to Fig. S9A) to generate with proportional adjustments to other state occupancies to maintain a total of 1 for all states at equilibrium ('starting rates', Fig. S9B). To model pausing, we set pause entry to state A at 100 s^{-1} competing with pause bypass to 'after pause' at 50^{-1} (pause efficiency 67%), and allowed the other rates to float with fixed forward and reverse ratios to maintain the relative stabilities of states A–F (Fig. S9B). Using least-squares fitting in Kintek Explorer,(17) the multistate model fit the biphasic escape profile well with arbitrary forward–reverse rates of (A-to-B) 2.44 s^{-1}–0.468 s^{-1}, (B-to-C) 225 s^{-1}–588 s^{-1}, (C-to-D) 0.946 s^{-1}–7.3 s^{-1}, (D-to-E) 4.37 s^{-1}–0.152 s^{-1}, (E-to-F) 95.1 s^{-1}–46.5 s^{-1} and D-to-pause escape 7.68 s^{-1} ('after fit', Fig. S9B). These rates allowed states A–F to equilibrate in ~40 s compared to the ~0.5 s for the starting rates. The slower equilibration is a necessary consequence of biphasic escape kinetics on the tens of seconds time scale. Changes to the stabilities (G^0) of states B and F by factors of 5 were accomplished by changing B-to-C reverse to 118 s^{-1} or E-to-F reverse to 9.3 s^{-1} (Fig. 7C; Fig. S9B).

Data availability

Cryo-EM data have been deposited in the RCSB Protein Data Bank (www.pdb.org) and in the Electron Microscopy Data Bank (www.emdatabank.org). The PDB accession codes for the coordinates of ePEC-1, con-ePEC-fTL, con-ePEC-uTL *his*-ePEC_fTL_Fin_1, *his*-ePEC_fTL_Fin_2, *his*-ePEC_fTL_Fout, *his*-ePEC_ufTL_1, *his*-ePEC_ufTL_2 are 8EG7, 8EG8, 8EGB, 8EH8, 8EH9, 8EHA, 8EHF, and 8EHI, respectively, and the accession codes for the cryo-EM maps are EMD codes 28109, 28110, 28113, 28143, 28144, 28145, 28146, 28148.

Abbreviations used in main text and supplement

asRNA, antisense RNA; BH, bridge helix; cryoEM, cryogenic electron microscopy, CSSC, cystamine; CTR, Cys-triplet reporter; CPR, Cys-pair reporter; DTT, dithiothreitol; EC, elongation complex; EB, Elongation buffer; EDTA, ethylenediaminetetraacetic acid; IPTG; isopropyl β-D-1-thiogalactopyranoside; LDS, lithium dodecyl sulfate; NAC, nucleotide addition cycle; nt, nucleotide; NTP, nucleoside triphosphate; PAGE, polyacrylamide gel electrophoresis; PEC, paused elongation complex; ePEC, elemental paused elongation complex; hsPEC, hairpin-stabilized paused elongation complex; *his*PEC, paused EC formed in the *E. coli his* operon leader region – an hsPEC that forms an ePEC when the hairpin is absent; PEI, polyethylenimine; PMSF, phenylmethylsulfonyl fluoride; RH, rim helices; RNAP, RNA polymerase; SBHM, sandwich-barrel hybrid motif; SDS, sodium dodecyl sulfate; SI1, sequence insertion 1 in *E. coli* RNAP; SI3, sequence insertion 3 in *E. coli* RNAP; SPB, SI3 positional bias; TH, trigger helix; TL, trigger loop.

Table S1. *E. coli* RNAP structural modules.

RNAP structural module	subunit	residues
Core	αI, αII β β′ ω	all 1-27; 142-152; 445-455; 520-646; 704-713; 786-828; 1060-1240 343-368; 421-636 all
Swivel	β β′	1241-1342 1-342; 369-420; 787-930; 1135-1407
Clamp	β β′	1319-1342 1-342; 1318-1344
Dock	β′	369-420
Rim helices (RH)	β′	647-703
F-loop (FL)	β′	741-766
Bridge helix (BH)	β′	769-803
Shelf	β′	787-931; 1135-1317
Trigger loop (TL)	β′	903-944; 1133-1137
SI3	β′	945-1132
Jaw	β′	1151-1215

Table S2. Oligonucleotides and plasmids.

Oligonucleotides (5′ ➔ 3′)	**Assay**	**Stock #**
cryoEM, *con*-ePEC, non-template strand DNA GCGTCCGGTCGATCTTCGCCCGTAAATTCAGA	cryo-EM, pause assay	#10928
cryoEM, *con*-ePEC, template strand DNA TCTGAATTTACGGGCGCAACTATGCCGGACGC	cryo-EM, pause assay, Nun assay	#10930
cryoEM, *con*-ePEC, RNA, active reconstitution UUUUUUGGCAUAGUUG	cryo-EM, pause assay, Nun assay	#8401
con-ePEC, RNA, direct reconstitution UUUUUUGGCAUAGUUGC	pause assay	#8374
cryoEM, *his*-ePEC, non-template strand DNA GCGTCCTATCGATCTTCGGAAGAGATTCAGAG	cryo-EM, pause assay	#10924
cryoEM, *his*-ePEC, template strand DNA CTCTGAATCTCTTCCAGCACACATCAGGACGC	cryo-EM, pause assay, Nun assay	#10919
cryoEM, *his*-ePEC, RNA, direct reconstitution UCAUCCGGCGAUGUGUGCU	cryo-EM, pause assay	#8857
his-ePEC, RNA, active reconstitution UCAUCCGGCGAUGUGUGC	pause assay, Nun assay	#12192
con-ePEC scaffold2, non-template strand DNA GGTCAGTACGTCCGGCATAGTTGCGCCCGTAAATTCAGATCTTCCAGTGG	pause assay, CTR xlink assay	#9563
con-ePEC scaffold2, template strand DNA CCACTGGAAGATCTGAATTTACGGGCGCAACTATGCCGGACGTACTGACC	pause assay, CTR xlink assay	#8334
con-ePEC scaffold2, RNA UUUUUUGGCAUAGUU	pause assay, CTR xlink assay	#8342
his-ePEC scaffold2, non-template strand DNA GGTCAGTACGTCCTGCGATGTGTGCTGGAAGAGAATTCAGATCTTCCAGT	pause assay, CTR xlink assay	#14074
his-ePEC scaffold2, template strand DNA ACTGGAAGATCTGAATTCTCTTCCAGCACACATCGCAGGACGTACTGACC	pause assay, CTR xlink assay	#14073
his-ePEC scaffold2, RNA GUCAUCCGGCGAUGUGUG	pause assay, CTR xlink assay	#12644
his-ePEC scaffold2, antisense RNA CCGGAUGA	pause assay, CTR xlink assay, Nun assay	#6598
con-ePEC scaffold3, non-template strand DNA GCGTCCGGCATAGTTGCGCCCGTAAATTCAGA	Nun assay	#12641
his-ePEC scaffold3, non-template strand DNA GCGTCCTGATGTGTGCTGGAAGAGATTCAGAG	Nun assay	#12642

Plasmids	**Source**	**Stock #**
pRM756 *Eco*RNAP (*E. coli* $\alpha_2\beta\beta'\omega$) overexpression plasmid containing his10-ppx tag at β′ C-terminus	(18)	#2956
pRM843 *Eco*RNAP ($\alpha_2\beta\beta'\omega$) overexpression plasmid containing HMK-Strep tag at rpoC C-terminus and his10-ppx tag at β N-terminus	(19)	#5143
p*EcrpoA*(-$X_{234–241}$H)*BCZ*	(1)	–
pACYCDuet-1*rpoZ*	(2)	–
pYB101 CPR(SI3–RH): *Eco*RNAP ($\alpha_2\beta\beta'\omega$) overexpression plasmid containing his10-ppx tag at β′ C-terminus, plus β′D1051C and β′G671C substitutions	(3)	#6351
pRM1213 CTR: *Eco*RNAP ($\alpha_2\beta\beta'\omega$) overexpression plasmid containing HMK-Strep tag at β′ C-terminus and his10-ppx tag at β N-terminus, plus βR267C, β′D1051C and β′G671C substitutions	(3)	#6013

Table S3. Cryo-EM data acquisition and refinement parameters.

Sample	ePEC-1	ePEC	
Class		ePEC_fTL	ePEC_ufTL
EMDB	EMD-28109	EMD-28110	EMD-28113
PDB	8EG7	8EG8	8EGB
Data collection and processing			
Microscope	Titan Krios	Titan Krios	
Voltage (kV)	300	300	
Detector	K2 Summit	K2 Summit	
Electron exposure (e–/Å^2)	47.5	47.5	
Defocus range (μm)	-0.8 - -2.4	-0.8 - -2.4	
Data collection mode	Super-resolution	Super-resolution	
Pixel size (Å)	1.3 (after binning)	1.3 (after binning)	
Symmetry imposed	C1	C1	
Initial particle images (no.)	666,501	716,722	
Final particle images (no.)	213,041	197,891	162,844
Map resolution (Å) - FSC threshold 0.143	3.2	3.3	3.8
Refinement[c]			
Initial model used (PDB code)	6ALF[a]	6ALF[a]	6ALF[a]
Map sharpening B factor (Å^2)	-69.93	-96.14	-128.47
Model composition			
Non-hydrogen atoms	26,200	26,553	26,419
Protein residues	3,174	3,219	3,197
Nucleic acid residues	65	67	69
	1 Mg^{2+}	1 Mg^{2+}	1 Mg^{2+}
	2 Zn^{2+}	2 Zn^{2+}	2 Zn^{2+}
Ligands	2 CHAPSO	2 CHAPSO	2 CHAPSO
B factors (Å^2)			
Protein	56.46	48.05	75.96
Nucleic acid	122.43	80.84	103.83
Ligands	57.50	46.23	72.06
R.m.s. deviations			
Bond lengths (Å)	0.004	0.003	0.003
Bond angles (°)	0.594	0.585	0.596
Validation			
MolProbity score	2.16	1.67	1.72
Clashscore	8.67	5.44	6.97
Poor rotamers (%)	2.52	3.23	3.35
Ramachandran plot			
Favored (%)	94.3	94.48	95.12
Disallowed (%)	0	0	0.03

Table S3, continued

Sample			*his*-ePEC		
Class	*his*-ePEC_ufTL_1	*his*-ePEC_ufTL_2	*his*-ePEC_fTL-Fout	*his*-ePEC_fTL-Fin_1	*his*-ePEC_fTL-Fin_2
EMDB	EMD-28146	EMD-28148	EMD28145	EMD-28143	EMD-28144
PDB	8EHF	8EHI	8EHA	8EH8	8EH9
Data collection and processing					
Microscope			Titan Krios		
Voltage (kV)			300		
Detector			K2 Summit		
Electron exposure (e–/Å^2)			47.5		
Defocus range (μm)			-0.8 - -2.4		
Data collection mode			Super-resolution		
Pixel size (Å)			1.3 (after binning)		
Symmetry imposed			C1		
Initial particle images (no.)			1,937,183		
Final particle images (no.)	432,336	210,600	58,000	151,000	30,000
Map resolution (Å) - FSC threshold 0.143	3.3	5.5	3.7	3.4	3.9
Refinement[c]					
Initial model used (PDB code)	6ALF[a]	6ALF[a]	6ALF[a]	6ALF[a]	6ALF[a]
Map sharpening B factor (Å^2)	-88.31	-303.14	-65.53	-81.02	-88.31
Model composition					
Non-hydrogen atoms	26,110	26,073	26,249	26,245	26,233
Protein residues	3,170	3,170	3,190	3,190	3,190
Nucleic acid residues	63	63	64	64	64
	1 Mg^{2+}	1 Mg^{2+}	1 Mg^{2+}	1 Mg^{2+}	1 Mg^{2+}
	2 Zn^{2+}	2 Zn^{2+}	2 Zn^{2+}	2 Zn^{2+}	2 Zn^{2+}
Ligands	1 CHAPSO		1 CHAPSO	1 CHAPSO	1 CHAPSO
B factors (Å2)					
Protein	53.97	232.3	60.37	45.38	49.37
Nucleic acid	146.27	261.4	105.99	95.07	92.15
Ligands	40.87	294.5	48.33	34.17	35.14
R.m.s. deviations					
Bond lengths (Å)	0.005	0.003	0.004	0.003	0.003
Bond angles (°)	0.681	0.702	0.611	5.83	0.745
Validation					
MolProbity score	2.25	2.31	2.24	2.24	1.87
Clashscore	7.04	8.83	6.93	7.33	8.64
Poor rotamers (%)	3.82	3.34	3.73	3.77	3.89
Ramachandran plot					
Favored (%)	93.56	93.33	93.64	94.17	94.05
Disallowed (%)	0.03	0.19	0.00	0.00	0.00

[a]Kang et al., 2018 (20)

Table S4. EC and PEC structures, states, and conformational features.

Structure	# particles	%	%	Res (Å)	Fig. 7 state - name	TL	Transl	RH-F	Swivel
ePEC$_{-1}$	213K		100	3.2	–	uf	Post	up	no
con-ePEC-fTL	198K		55	3.3	B fTL-Fin1	f	Pre	down	no
con-ePEC-ufTL	163K		45	3.8	D ufTL-Fout	uf	Pre	up	yes
his-ePEC-fTL-Fout	58K	6.6	27	3.7	C fTL-Fout	f	Pre	up	no
his-ePEC-fTL-Fin1	151K	17		3.4	B fTL-Fin1	f	Pre	down	no
his-ePEC-fTL-Fin2	30K	3.4		3.9	A fTL-Fin2	f	Pre	tight	no
his-ePEC-ufTL2	212K	24	73	5.5	E ½-swiveled	uf	1/2	up	1/2
his-ePEC-ufTL1	434K	49		3.3	F swiveled	uf	1/2	up	yes

Table S5. Half-map analysis of swivel angles.

structure	# particles	res.(Å)	map	swivel
con-ePEC$_{-1}$	213K	3.2	full	0.82°
			half map analysis	1.0° ± 0.3°
con-ePEC_fTL	198K	3.3	full	(0°)
con-ePEC_ufTL	163K	3.8	full	0.86°
			half map analysis	1.2° ± 0.4°
his-ePEC_fTL-Fout	58K	3.7	full	(0°)
his-ePEC_fTL-Fin1	151K	3.4	full	(0°)
his-ePEC_fTL-Fin2	30K	3.9	full	(0°)
his-ePEC_ufTL2	212K	5.5	full	2.3°
			half map analysis	2.3° ± 0.2°
his-ePEC_ufTL1	434K	3.3	full	3.8°
			half map analysis	3.6° ± 0.2°

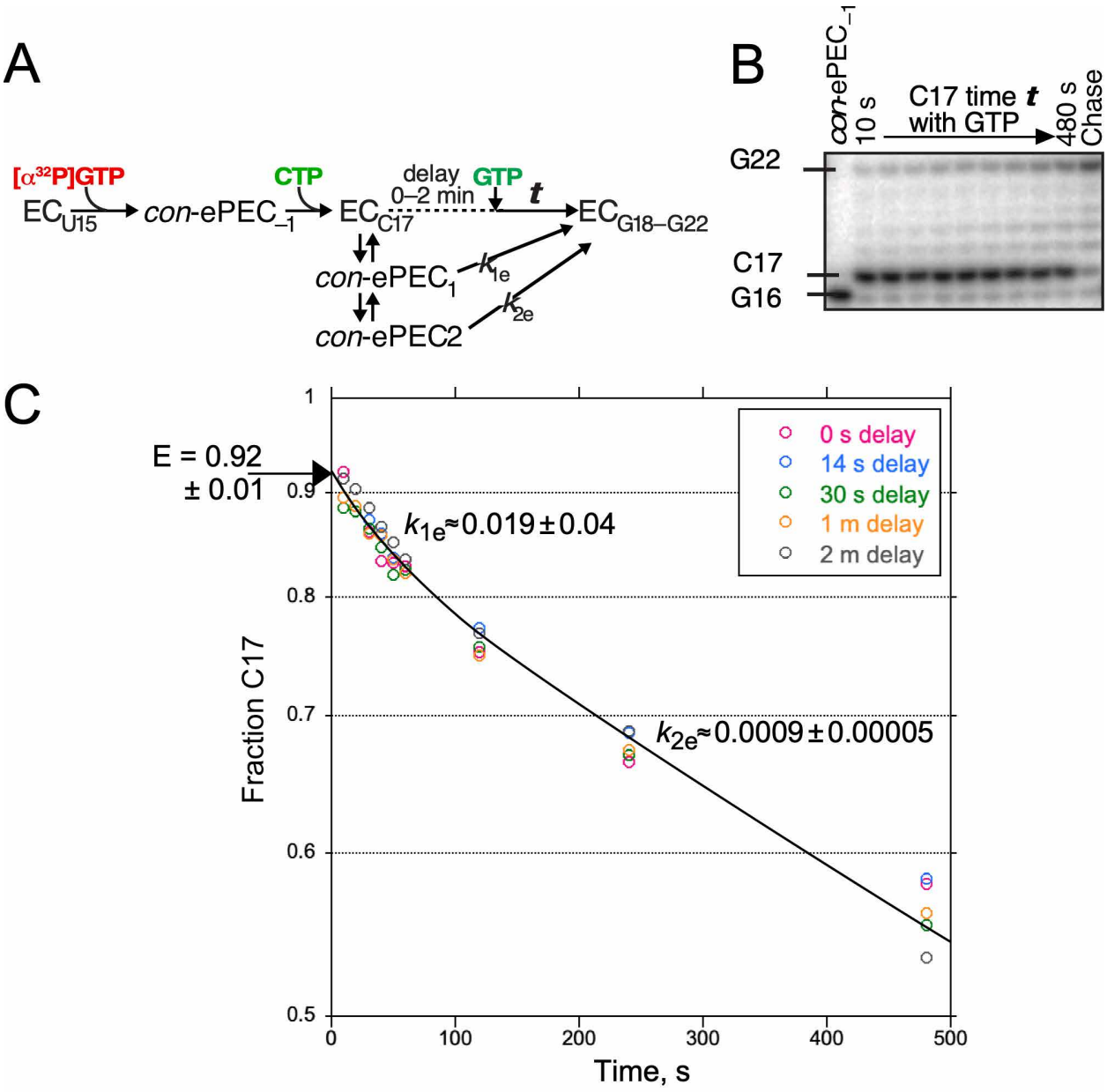

Figure. S1. ***Con*-ePECs rapidly equilibrate between various translocation states following nucleotide addition.** (A) Experimental scheme for measuring pause escape following various incubation times at the pause. Starting *con*-ePEC$_{-1}$ complexes containing 5'-^{32}P G16 RNA were incubated at 23 ºC with CTP, the nucleotide that positions RNAP at the pause upon addition. Following reaction with CTP for the indicated amount of time, *con*-ePECs were allowed to escape the pause in the presence of GTP (10 μM) at 23 ºC. (B) A representative urea-PAGE gel of the *con*-ePEC reaction at 23 ºC with GTP (10 μM), the nucleotide necessary for escape from the pause. (C) Quantitation of pause RNA fraction (C17) at increasing GTP addition delay times showing invariable y-intercept of pause decay kinetics, indicative of the fraction of complexes entering the pause.

.

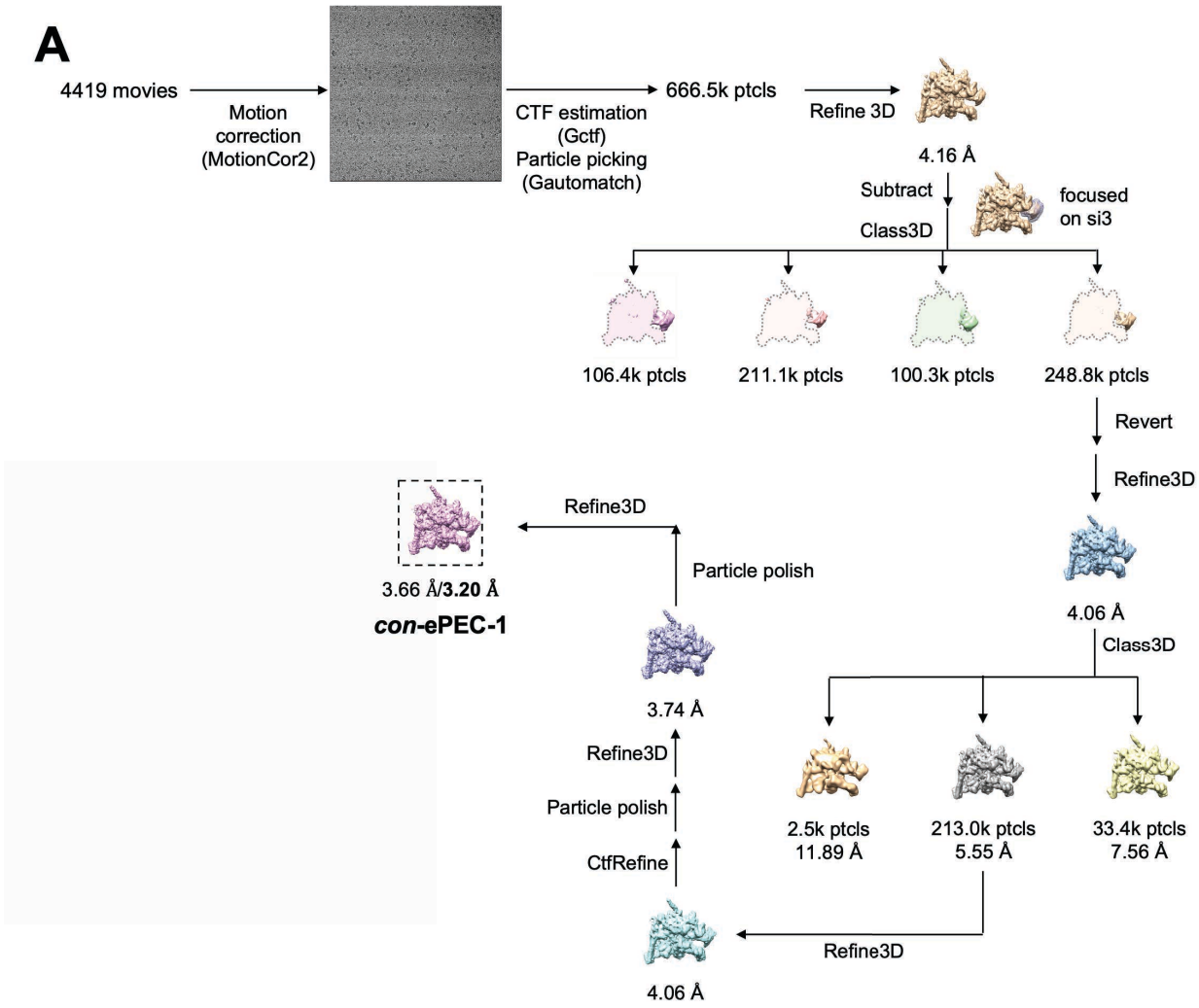

Fig. S2. **Cryo-EM processing for *con*-ePEC-1 and *con*-ePEC. Note: Fig. S2 and Fig. S2 legend continues on following pages. (A)** cryo-EM processing pipeline for *con*-ePEC-1. **(B)** cryo-EM processing pipeline for *con*-ePEC and map nomenclature. **(C)** Gold-standard Fourier-shell correlation (FSC) plot for *con*-ePEC-1 (orange), *con*-ePEC_fTL (dark blue), and *con*-ePEC_ufTL(yellow). The FSCs are calculated by comparing the independently determined half-maps from RELION. The dotted line represents the 0.143 FSC cutoff which indicates a nominal resolution the maps. **(D–F)** The cryo-EM maps filtered by local resolution (21) are shown. The view on the right is a cross-section. (top) Colored by subunit as follows - β′: pink, β: cyan, light yellow: SI3, red: rim helices, gray: the rest part of the map. (bottom) Colored by local resolution (key on the bottom). **(D)** *con*-ePEC-1. **(E)** *con*-ePEC_fTL. **(F)** *con*-ePEC-ufTL. **(G–I)** Particle orientation distribution (top) is calculated from the refinement run in RELION, and the directional 3D FSC is calculated by 3DFSC (bottom) (22). **(G)** *con*-ePEC-1. **(H)** *con*-ePEC_fTL. **(I)** *con*-ePEC-ufTL.

Figure S2, continued.

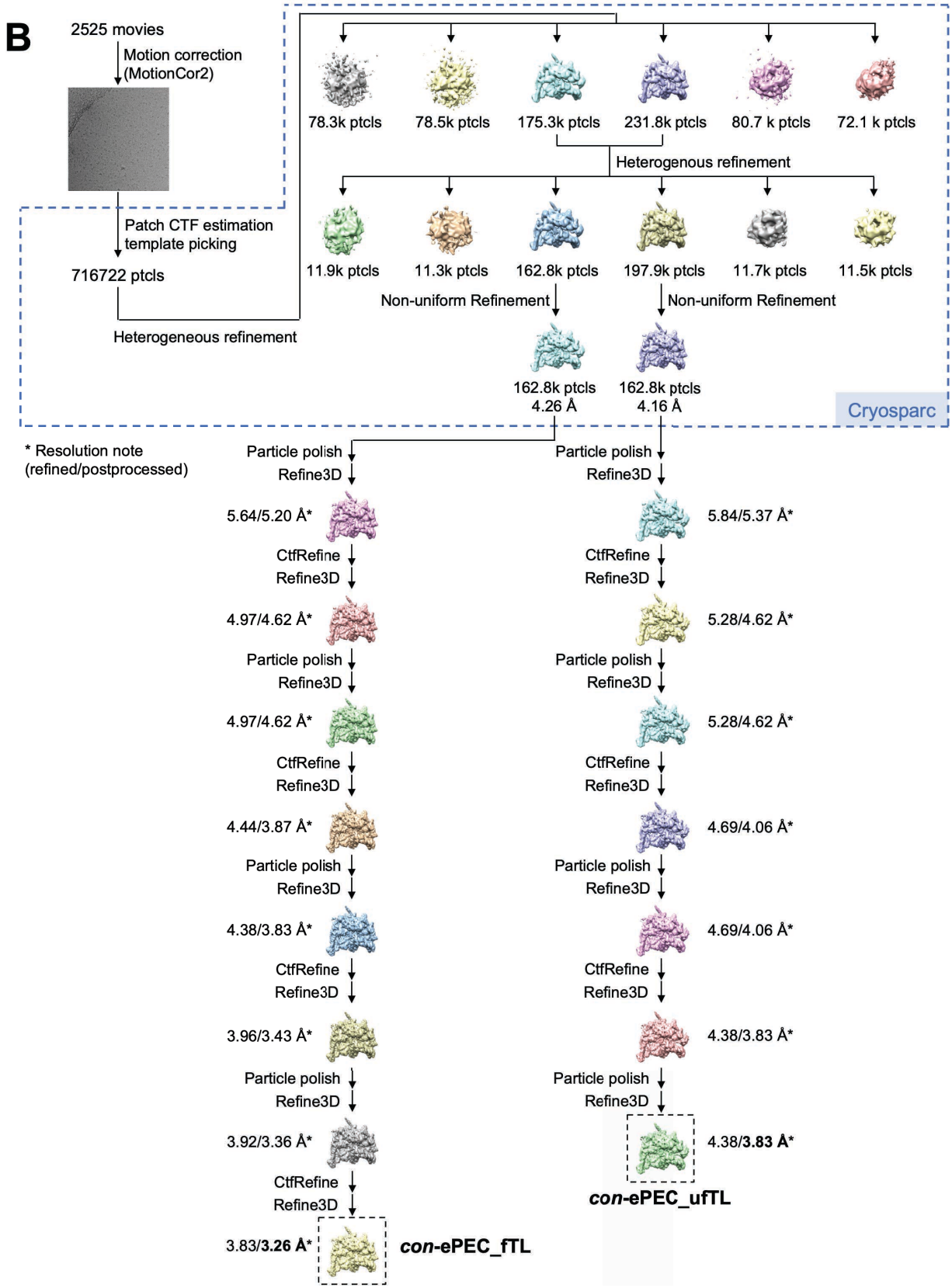

Fig. S2 . Cryo-EM processing for *con*-ePEC-1 and *con*-ePEC, continued. (B) cryo-EM processing pipeline for *con*-ePEC and map nomenclature.

Figure S2, continued.

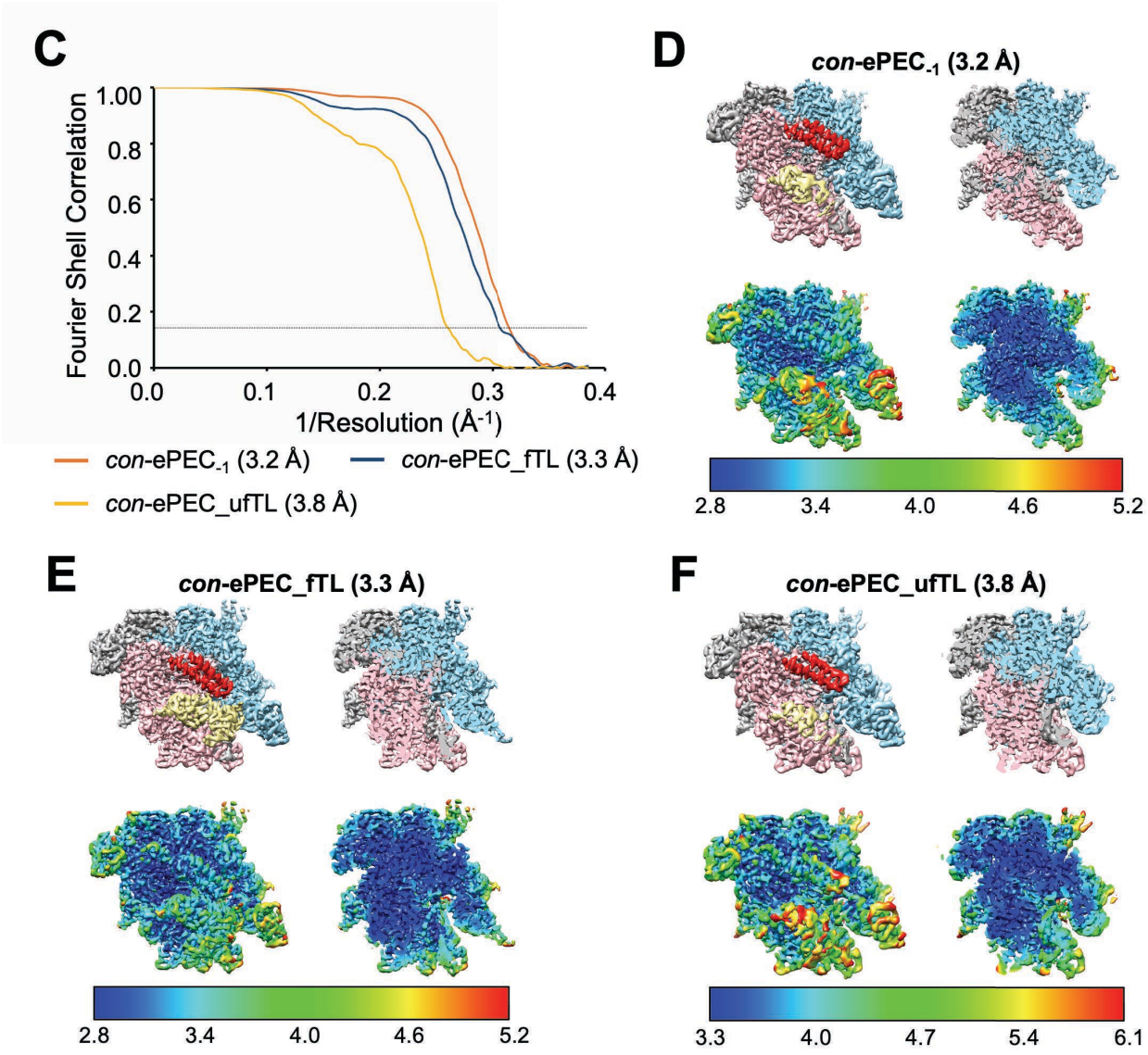

Fig. S2 . **Cryo-EM processing for *con*-ePEC-1 and *con*-ePEC, continued. (B)** cryo-EM processing pipeline for *con*-ePEC and map nomenclature. **C)** Gold-standard Fourier-shell correlation (FSC) plot for *con*-ePEC-1 (orange), *con*-ePEC_fTL (dark blue), and *con*-ePEC_ufTL(yellow). The FSCs are calculated by comparing the independently determined half-maps from RELION. The dotted line represents the 0.143 FSC cutoff which indicates a nominal resolution the maps. **(D–F)** The cryo-EM maps filtered by local resolution (21) are shown. The view on the right is a cross-section. (top) Colored by subunit as follows - β′: pink, β: cyan, light yellow: SI3, red: rim helices, gray: the rest part of the map. (bottom) Colored by local resolution (key on the bottom). **(D)** *con*-ePEC-1. **(E)** *con*-ePEC_fTL. **(F)** *con*-ePEC-ufTL

Figure S2, continued.

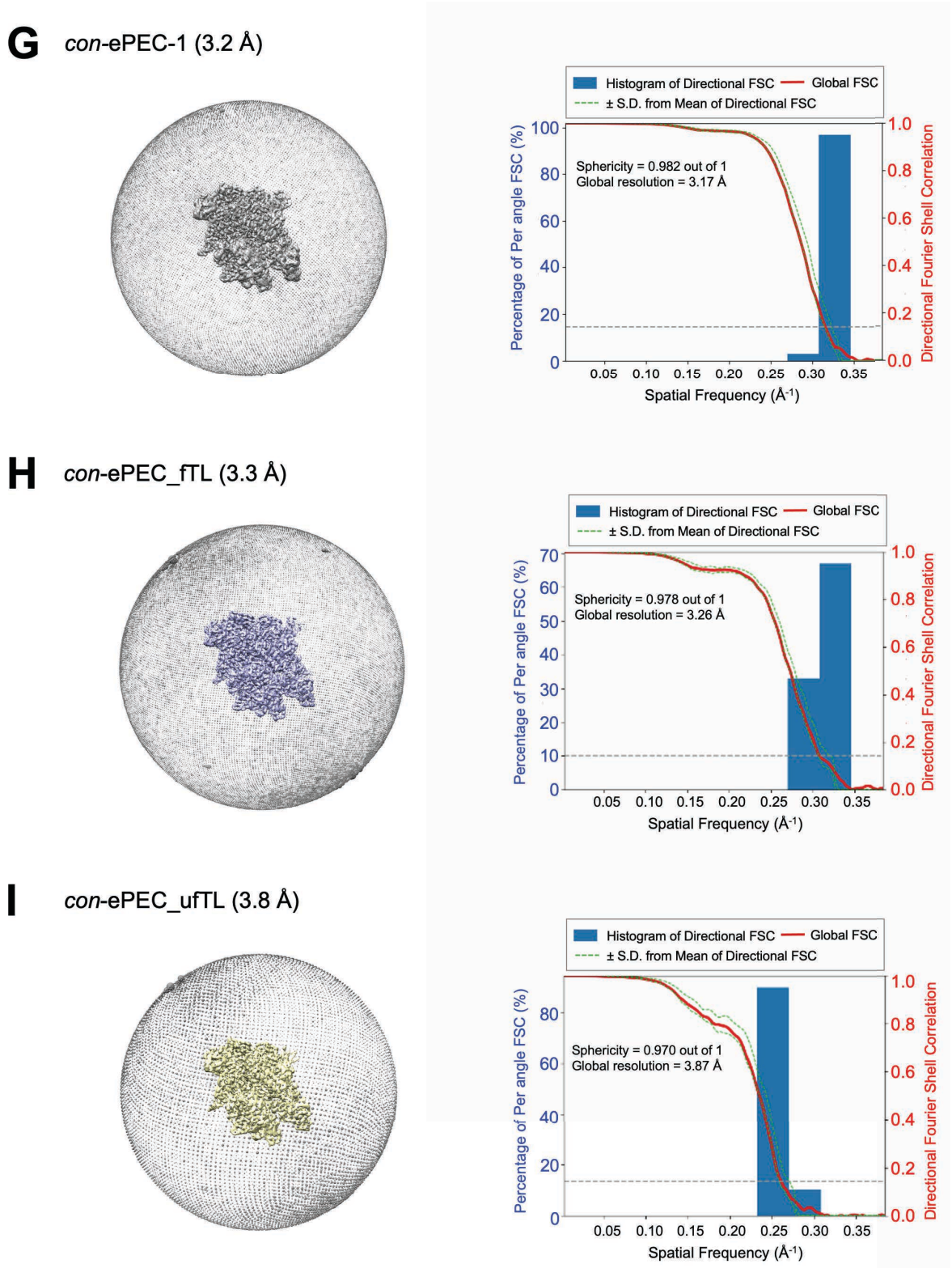

Fig. S2 . **Cryo-EM processing for *con*-ePEC-1 and *con*-ePEC, continued. (G–I)** Particle orientation distribution (top) is calculated from the refinement run in RELION, and the directional 3D FSC is calculated by 3DFSC (bottom) (22). **(G)** *con*-ePEC-1. **(H)** *con*-ePEC_fTL. **(I)** *con*-ePEC-ufTL

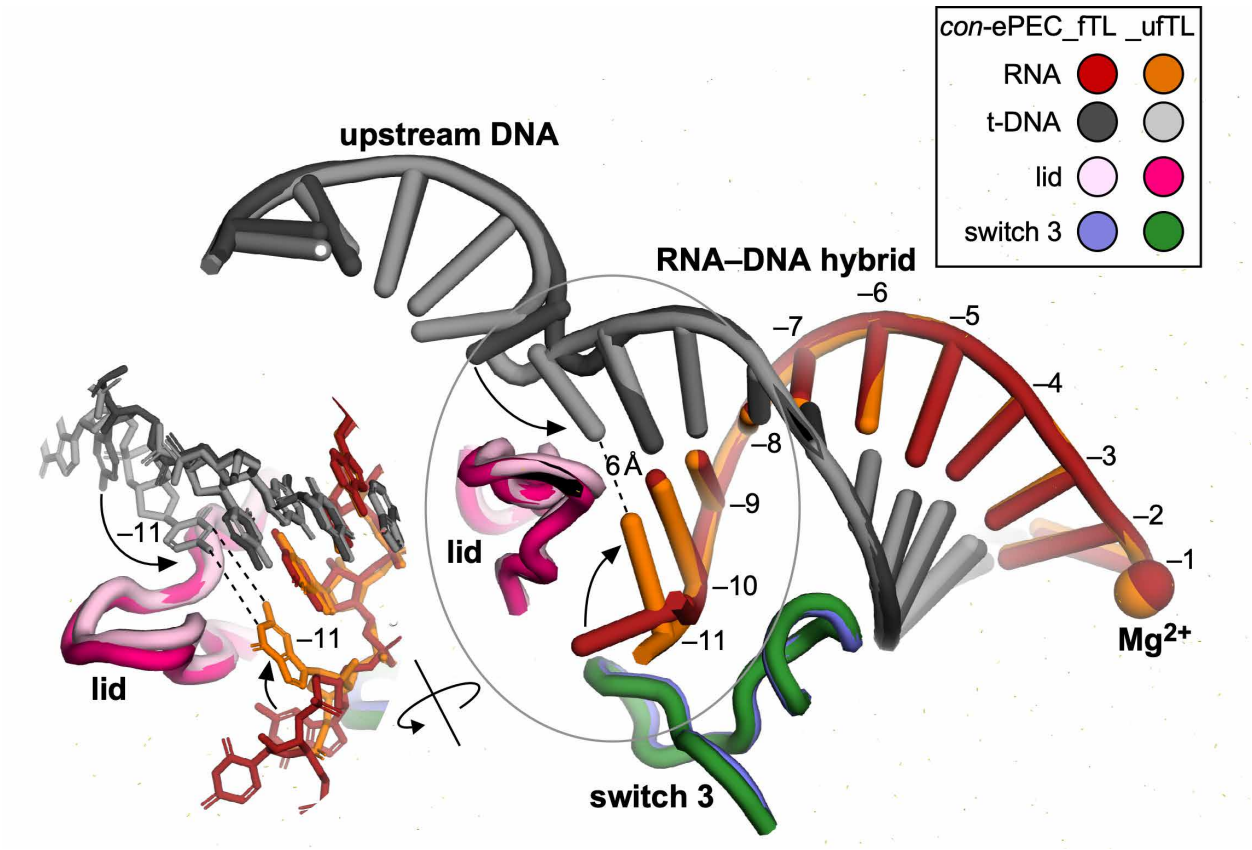

Fig. S3. The upstream fork junction of pre-translocated *con*-ePEC rearranges when the TL unfolds. In *con*-ePEC_fTL, nascent RNA –11 G interacts with switch 3 and t-DNA –11 C is paired to upstream nt-DNA –11 G. When the TL unfolds in the pretranslocated *con*-ePEC, t-DNA –11 C rotates back into the main cleft to approach nascent RNA –11 G. This interaction of –11 G with the tDNA in the main cleft of RNAP generates a 11-bp RNA–DNA hybrid, as also recently observed in a pretranslocated EC stabilized by interaction with *put* RNA (23). Formation of this –11 near-bp may stabilize the pretranslocated *con*-ePEC and explain the conservation of the strong –11 rG–dC bp in the consensus ePEC pause signal (Fig. 1B) (24, 25).

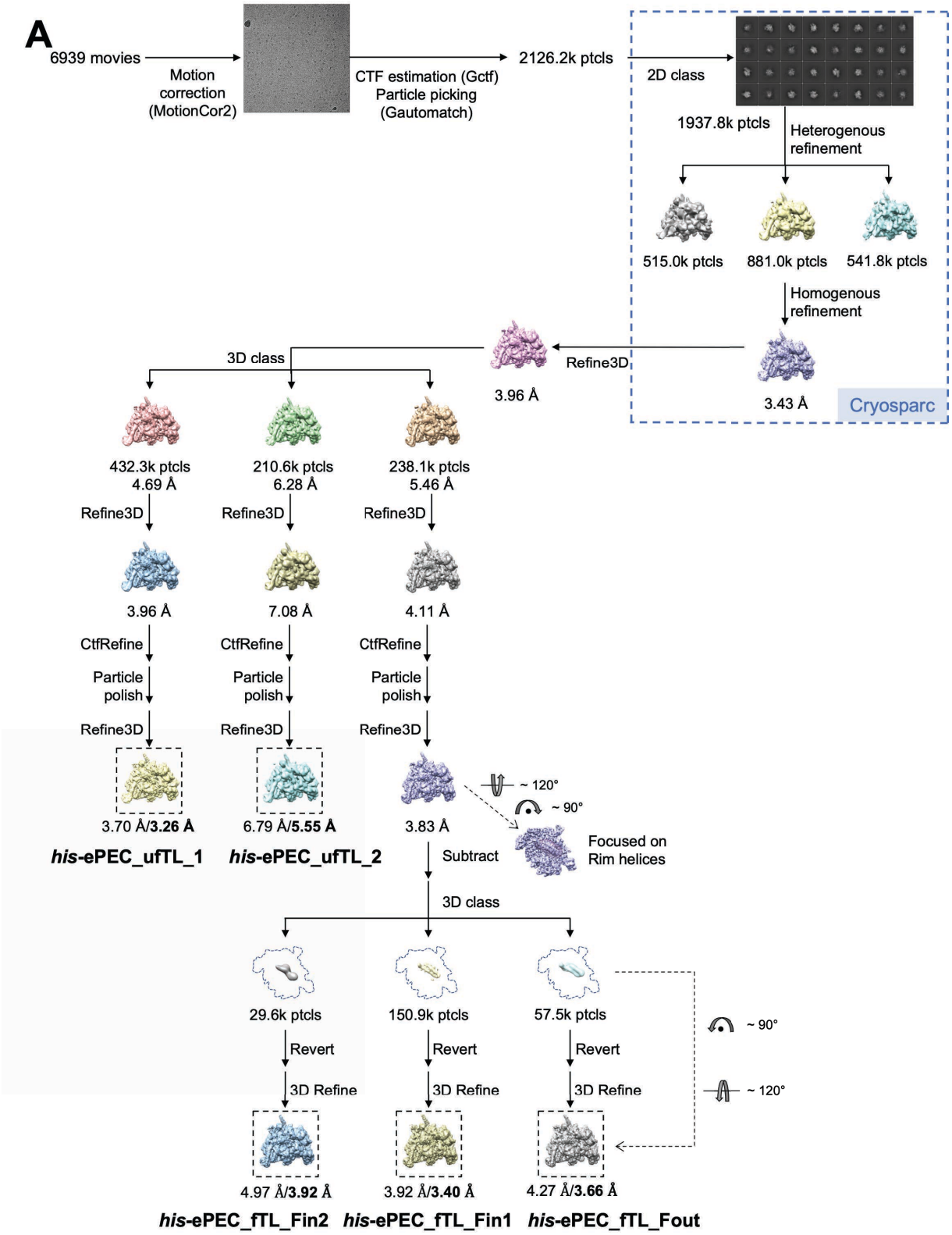

Fig. S4. Cryo-EM processing for *his*-ePEC. Note: Fig. S4 and S4 legend continues on following pages. (A) cryo-EM processing pipeline for *his*-ePEC and map nomenclature.

Figure S4, continued.

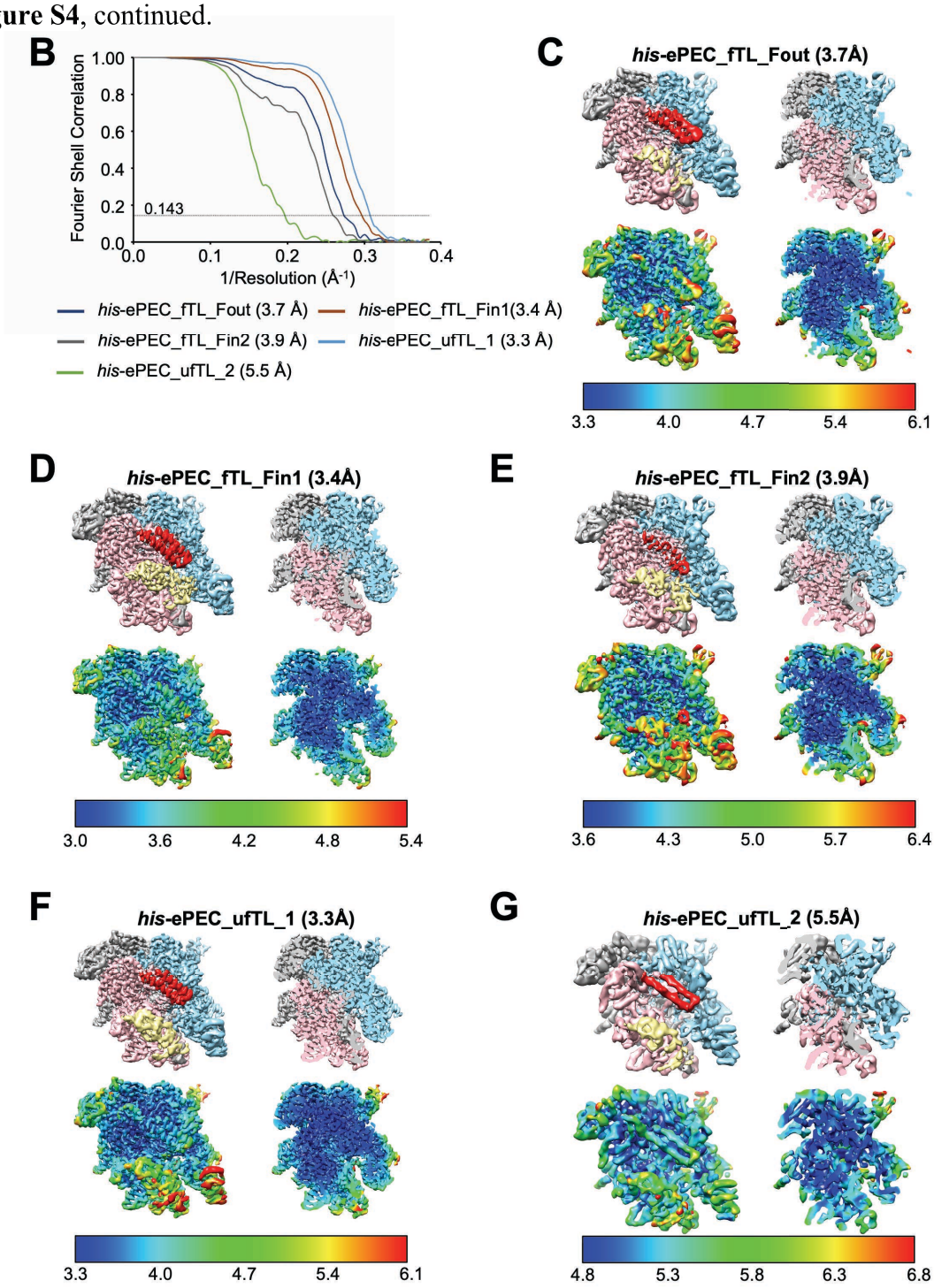

Fig. S4. Cryo-EM processing for *his*-ePEC, continued. (B) Gold-standard Fourier-shell correlation (FSC) plot for *his*-ePEC maps – *his*-ePEC_fTL_Fout (dark blue), *his*-ePEC_fTL_Fin1 (brown), *his*-ePEC_fTL_Fin2 (gray), *his*-ePEC_ufTL_1 (cyan), and *his*-ePEC_ufTL_2 (green). The FSCs are calculated by comparing the independently determined half-maps from RELION. The dotted line represents the 0.143 FSC cutoff which indicates a nominal resolution the maps. **(C–G)** The cryo-EM maps filtered by local resolution (21) are shown. The view on the right is a cross-section. (top) Colored by subunit as follows - β′: pink, β: cyan, light yellow: SI3, red: rim helices, gray: the rest part of the map. (bottom) Colored by local resolution (key on the bottom). **(C)** *his*-ePEC-fTL_Fout. **(D)** *his*-ePEC_fTL_Fin1. **(E)** *his*-ePEC-fTL_Fin2. **(F)** *his*-ePEC_ufTL_1. **(G)** *his*-ePEC_ufTL_2.

Figure S4, continued.

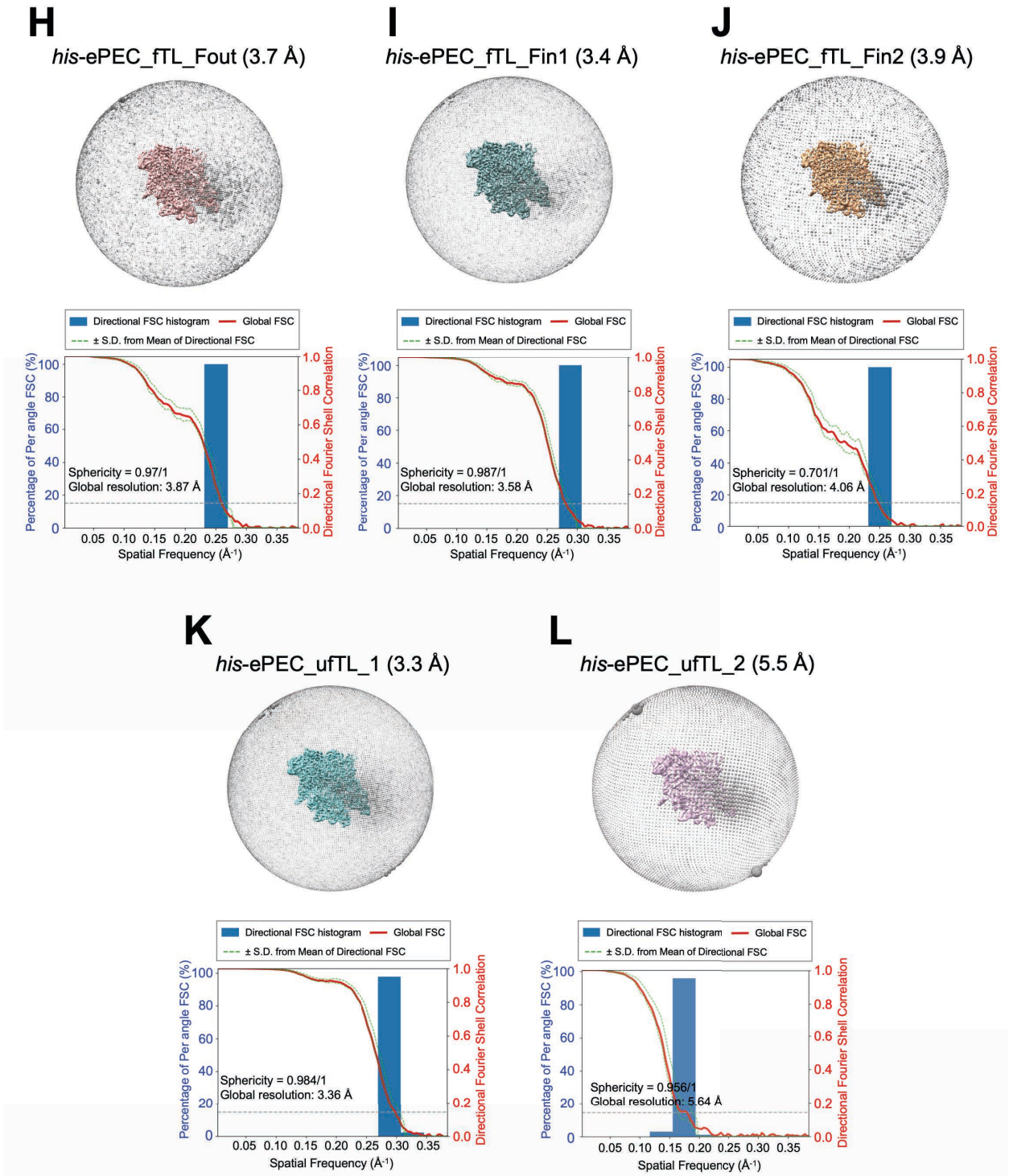

Fig. S4. **Cryo-EM processing for *his*-ePEC, continued. (H–L)** Particle orientation distribution (top) is calculated from the refinement run in RELION, and the directional 3D FSC is calculated by 3DFSC (bottom) (22). **(H)** *his*-ePEC-fTL_Fout. **(I)** *his*-ePEC_fTL_Fin1. **(J)** *his*-ePEC-fTL_Fin2. **(K)** *his*-ePEC_ufTL_1. (**L)** *his*-ePEC_ufTL_2.

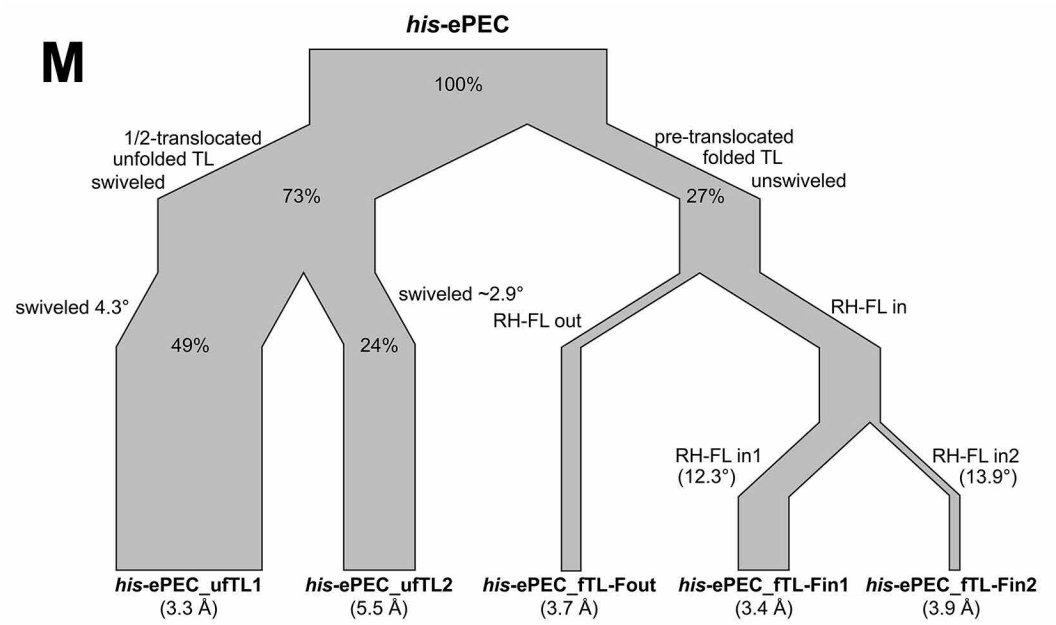

Fig. S4. **Cryo-EM processing for *his*-ePEC, continued. (M)** Particle-sorting dendrogram of *his*-ePEC conformations. The relative amounts of different *his*-ePEC states and their relationships during particle sorting are represented by the widths and junctions, respectively, of the dendrogram roots. The complete particle sorting analysis for *his*-ePEC is shown in Fig. S4A.

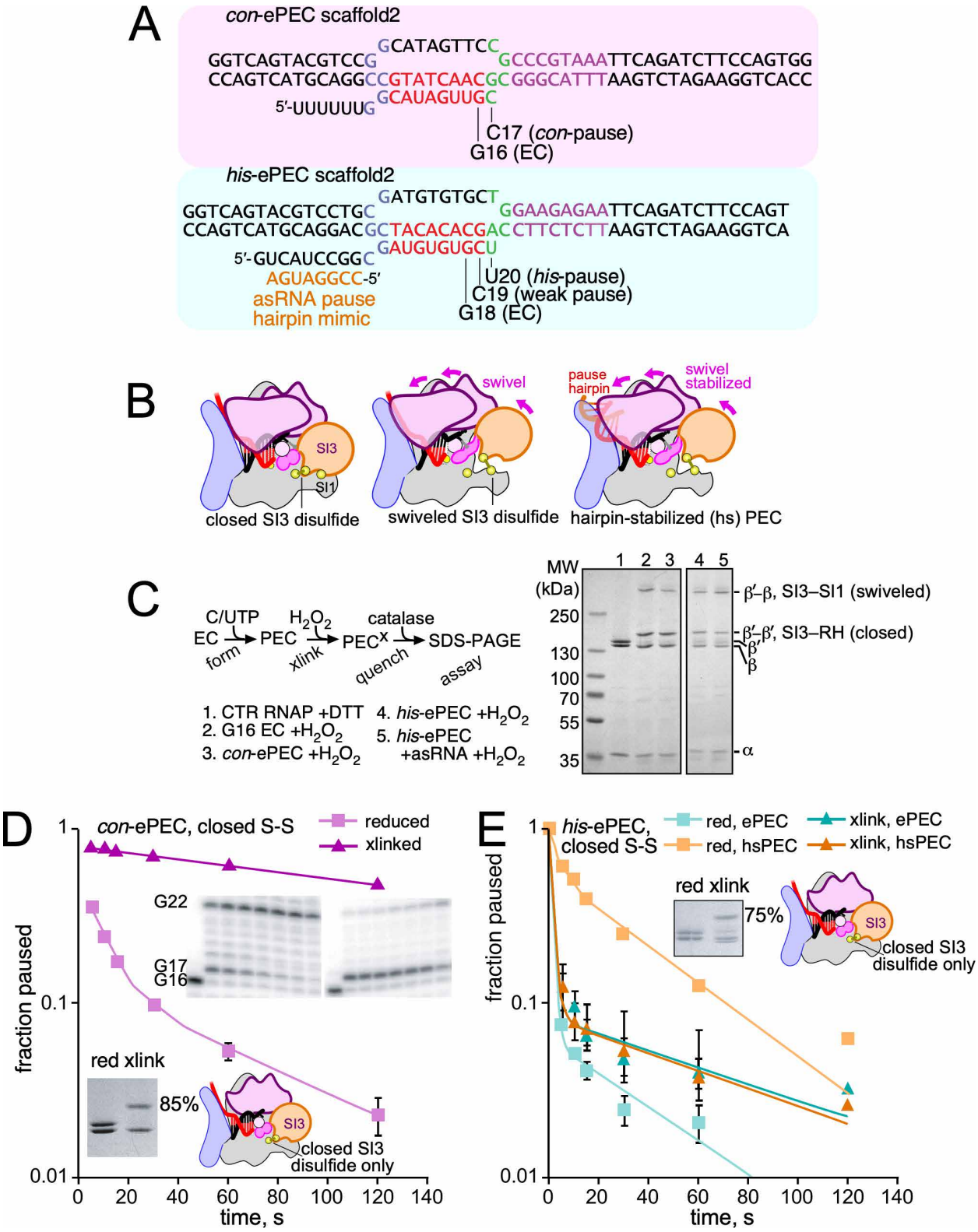

Fig. S5. Cys-triplet reporter analysis of ePEC conformations. (**A**) The scaffold sequences used for CTR and pausing assays of *con*-ePEC and *his*-ePEC. These scaffolds are fully complementary and contain sufficient duplex downstream DNA to avoid perturbing effects on translocation register

(B) Conformations of the EC and ePEC sampled during the CTR assay.
(**C**) The CTR assay (3). The representative gel panel shows relative migration in SDS-PAGE of the SI3–RH (β′–β′) and SI3–SI1 (β′–β′) crosslinks for samples listed by lane number. The RNAP diagrams depict relative Cys locations in SI3 closed, open, and swiveled states showing the swivel module for RNAP.
(**D**) Pausing kinetics of *con*-ePEC on the complete complementary scaffold (panel A) when the SI3–RH (closed) disulfide is formed using H_2O_2 or is reduced using DTT (see 3). The RNAP used for this experiment contained only two added Cys residues so the closed (SI3–RH) disulfide was formed exclusively. The insets show representative gel panels of the denaturing RNA gel for the pause assay and the extent of crosslinking assayed by SDS-PAGE. The strong increase in pausing when the crosslink is formed is consistent with a predominant role of the pre-translocated state for *con*-ePEC.
(**E**) Pausing kinetics of *his*-ePEC on the complete complementary scaffold (panel A) when the SI3–RH (closed) disulfide is formed or reduced as described for panel D. The minimal effect of the crosslink on pausing by *his*-ePEC compared to the strong inhibition pausing for the hairpin-stabilized *his*-PEC is consistent with a lesser role of the pre-translocated state for *his*-ePEC compared to *con*-ePEC (panel D). The *his*-ePEC results depicted here are replotted from data reported previously (3).

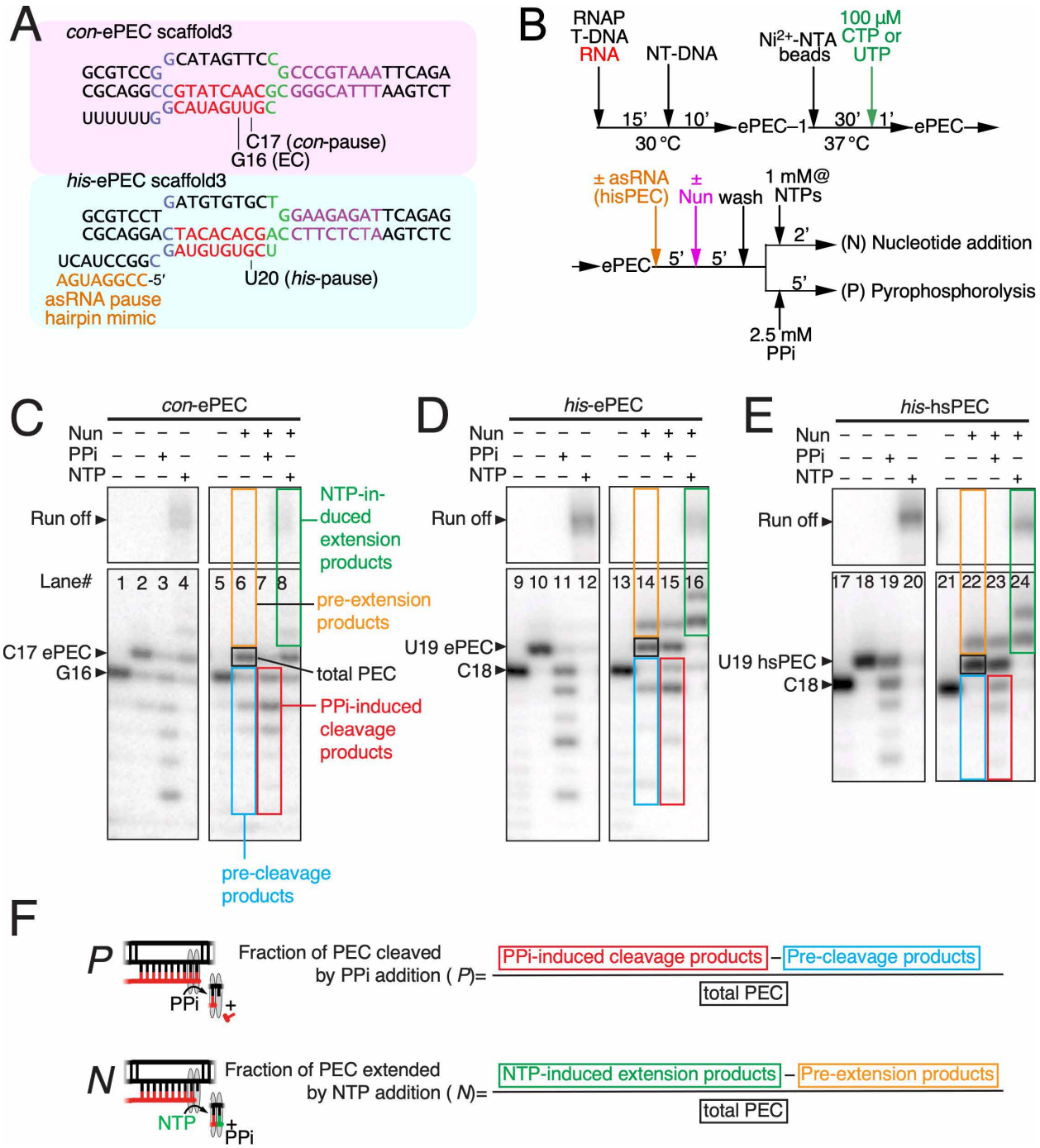

Fig. S6. Nun-locked catalysis assay of ePEC translocation register. (**A**) Scaffolds used for Nun-locked translocation assay. These scaffolds differ from those used for cryo-EM (Fig. 1B) only in being fully complementary to avoid any perturbing effects of fork-junction base-pairing equilibria on translocation register.

(**B**) Steps in the Nun-locked translocation assay.

(**C, D and E**) Gel images for Nun-locked translocation register assays with different scaffolds. The right panel of each image set (lanes 1−4, 9−12, 17−20) shows the NTP extension and pyrophosphorolysis species without Nun addition. Left panel of each image set: red boxes (lanes 7, 15, 23), shortened bands were induced by pyrophosphorolysis; green boxes (lanes 8, 16, 24),

extended bands were induced by NTP addition. Note that even without PPi/NTP addition (lanes 6, 14, 22), there are distinct species from PEC, possibly resulting from RNAP backtracking/autocleavage (blue boxes) and residual NTPs in Nun protein stock (orange boxes). These pre-reaction species were subtracted during quantitation to accurately calculate reaction products generated in Nun-locked complexes.
(**F**) Quantification formula for fraction of PEC cleaved by PPi addition (*P*) and fraction of PEC extended by NTP addition (*N*). Colors in the formula correspond to the boxes on the gel images.

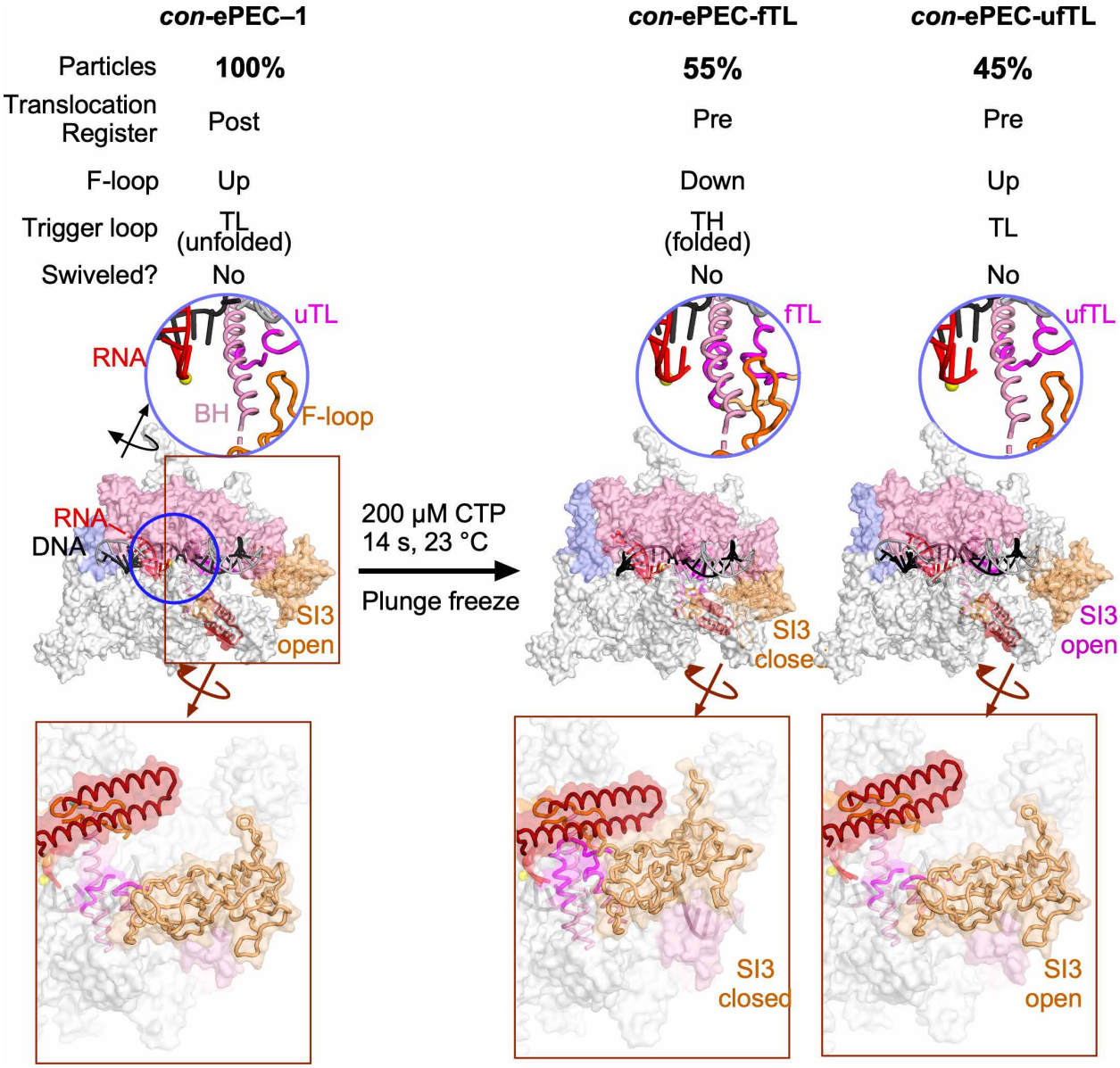

Fig. S7. Conformational changes in EC conversion to con-ePEC.

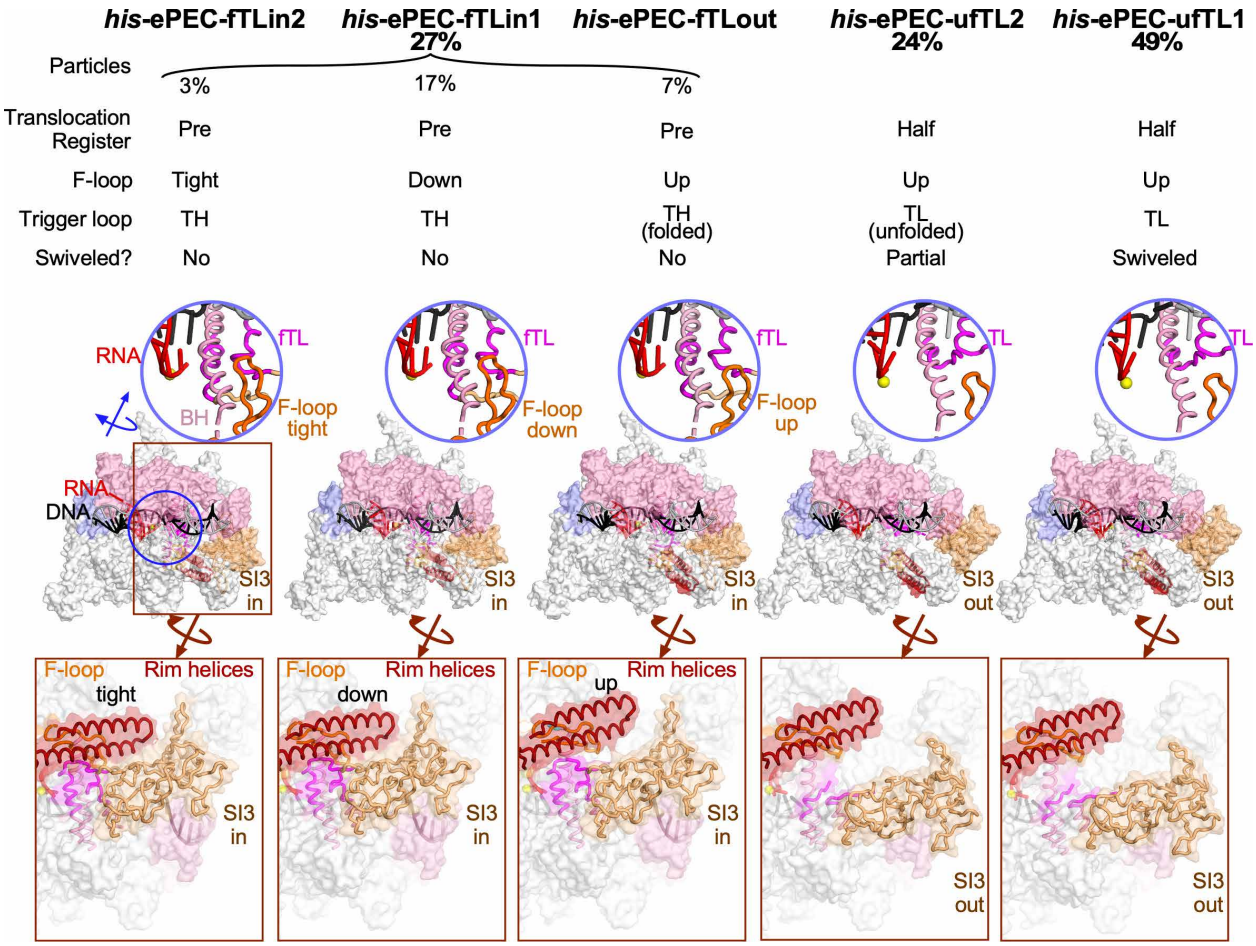

Fig. S8. Conformational states of the *his*-ePEC.

.

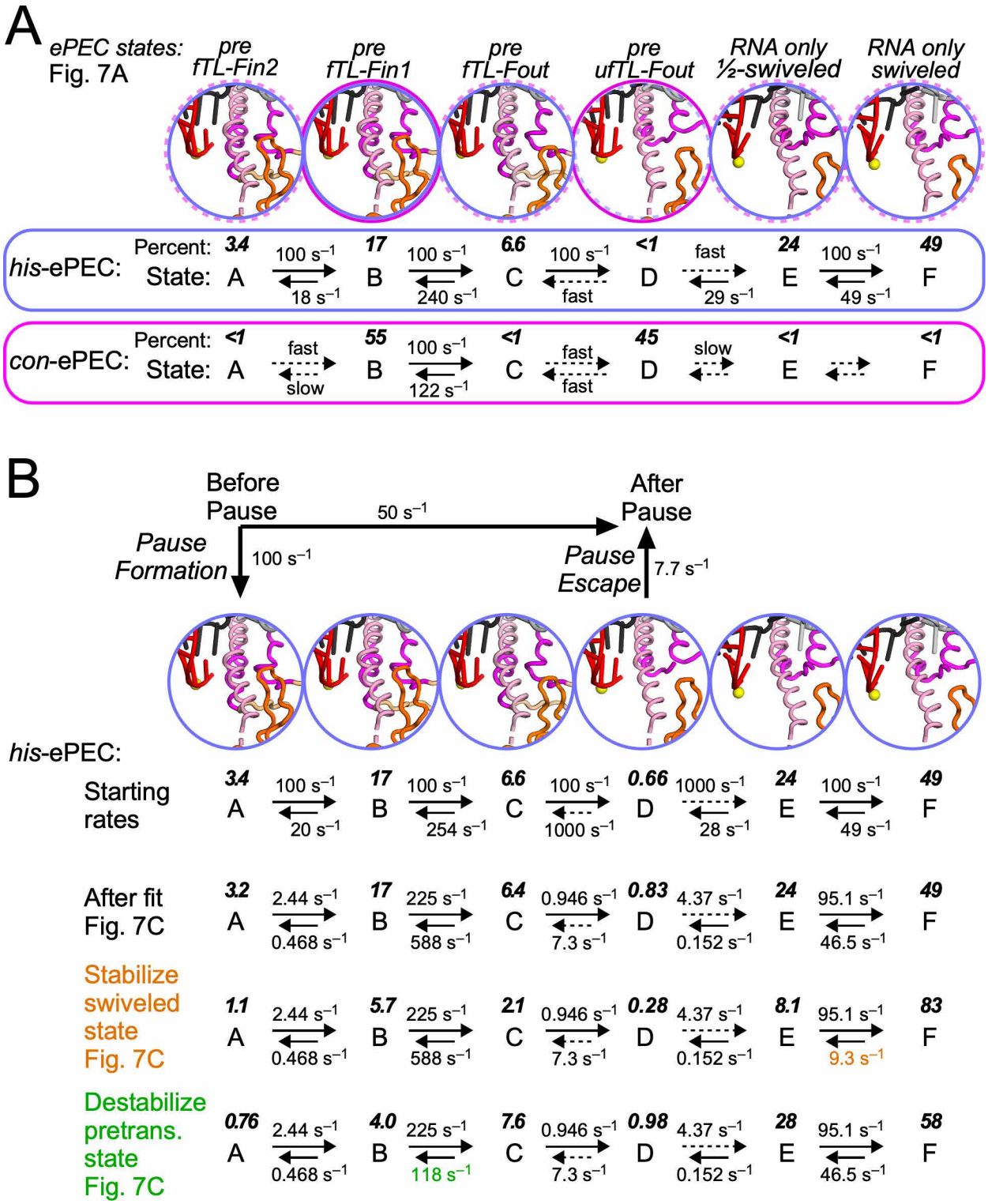

Fig. S9. Rate constants used for modeling distributions of ePEC states. The ePEC states correspond to those shown in Fig 7 and described in the text. The kinetic and thermodynamic modeling are described in the supplemental methods. Numbers in bold italics are the relative amounts of the states present at equilibrium when pause formation and escape rates are 0 and all RNAP is in an ePEC state (of 100 total).

A, distribution of states for *his*-ePEC (blue circles and oval) and for con-ePEC (magenta circles and oval). Circles with dashed lines represent states not observed by cryo-EM for *his*-ePEC or *con*-ePEC. We note that our modeling assumes all of the cryo-EM–detected states are paused, although it is possible that small amounts of active EC states could be intermixed in some of these populations. It is not feasible to identify these active EC fractions at currently achievable cryo-EM resolutions. Thus, we made the assumption at all states are fully paused to simplify the kinetic modeling.
B, modeling states for biphasic pausing kinetics. The rows with orange and green labels correspond to changes in rates shown in Fig. 7C. Note that the relative rates determine the distributions of states and are constrained by the fit to the structural data. However, the absolute rates, which are unknown, determine how fast equilibrium is reached and how fast states interconvert (see supplemental methods).

Legend to Supplemental Movie S1.

The movie shows the movements of active-site modules (BH, TL, RH, FL) and nucleic acids that connect the different elemental PEC states observed for *con*-ePEC and *his*-ePEC in two side-by-side views of the active site of RNAP. Movements of the BH, RH, and FL that accompany TL folding and unfolding are also likely to occur during the active NAC.

Supplemental References

1. Twist KA*, et al.* (2011) A novel method for the production of in vivo-assembled, recombinant Escherichia coli RNA polymerase lacking the alpha C-terminal domain. *Protein Sci* 20(6):986-995.
2. Bae B*, et al.* (2013) Phage T7 Gp2 inhibition of Escherichia coli RNA polymerase involves misappropriation of sigma70 domain 1.1. *Proc Natl Acad Sci U S A* 110(49):19772-19777.
3. Bao Y & Landick R (2021) Obligate movements of an active site-linked surface domain control RNA polymerase elongation and pausing via a Phe pocket anchor. *Proc Natl Acad Sci U S A* 118(36):e2101805118.
4. Chen J, Noble AJ, Kang JY, & Darst SA (2019) Eliminating effects of particle adsorption to the air/water interface in single-particle cryo-electron microscopy: Bacterial RNA polymerase and CHAPSO. *J Struct Biol X* 1.
5. Morin A*, et al.* (2013) Collaboration gets the most out of software. *Elife* 2:e01456.
6. Mastronarde DN (2005) Automated electron microscope tomography using robust prediction of specimen movements. *J Struct Biol* 152(1):36-51.
7. Zheng SQ*, et al.* (2017) MotionCor2: anisotropic correction of beam-induced motion for improved cryo-electron microscopy. *Nat Methods* 14(4):331-332.
8. Zhang K (2016) Gctf: Real-time CTF determination and correction. *J Struct Biol* 193(1):1-12.
9. Scheres SH (2012) RELION: implementation of a Bayesian approach to cryo-EM structure determination. *J Struct Biol* 180(3):519-530.
10. Punjani A, Rubinstein JL, Fleet DJ, & Brubaker MA (2017) cryoSPARC: algorithms for rapid unsupervised cryo-EM structure determination. *Nat Methods* 14(3):290-296.
11. Cardone G, Heymann JB, & Steven AC (2013) One number does not fit all: mapping local variations in resolution in cryo-EM reconstructions. *J Struct Biol* 184(2):226-236.
12. Kang JY*, et al.* (2018) Structural basis for transcript elongation control by NusG/RfaH universal regulators. *Cell* 173(7):1650-1662.e1614.
13. Pettersen EF*, et al.* (2004) UCSF Chimera--a visualization system for exploratory research and analysis. *J Comput Chem* 25(13):1605-1612.
14. Adams PD*, et al.* (2010) PHENIX: a comprehensive Python-based system for macromolecular structure solution. *Acta Crystallogr D Biol Crystallogr* 66(Pt 2):213-221.
15. Abdelkareem M*, et al.* (2019) Structural basis of transcription: RNA polymerase backtracking and its reactivation. *Mol Cell* 75(2):298-309 e294.
16. Marcoline FV, Furth J, Nayak S, Grabe M, & Macey RI (2022) Berkeley Madonna Version 10-A simulation package for solving mathematical models. *CPT Pharmacometrics Syst Pharmacol* 11(3):290-301.

17. Johnson KA, Simpson ZB, & Blom T (2009) Global kinetic explorer: a new computer program for dynamic simulation and fitting of kinetic data. *Anal Biochem* 387(1):20-29.

18. Windgassen T*, et al.* (2014) Trigger-helix folding pathway and SI3 mediate catalysis and hairpin-stabilized pausing by *Escherichia coli* RNA polymerase. *Nucleic Acids Res* 42(20):12707-12721.

19. Hein PP*, et al.* (2014) RNA polymerase pausing and nascent-RNA structure formation are linked through clamp-domain movement. *Nat Struct Mol Biol* 21(9):794-802.

20. Kang JY*, et al.* (2017) Structural basis of transcription arrest by coliphage HK022 nun in an Escherichia coli RNA polymerase elongation complex. *Elife* 6:e25478.

21. Heymann JB (2001) Bsoft: image and molecular processing in electron microscopy. *J Struct Biol* 133(2-3):156-169.

22. Tan YZ*, et al.* (2017) Addressing preferred specimen orientation in single-particle cryo-EM through tilting. *Nat Methods* 14(8):793-796.

23. Hwang S*, et al.* (2022) Structural basis of transcriptional regulation by a nascent RNA element, HK022 putRNA. *Nat Commun* 13(1):4668.

24. Imashimizu M*, et al.* (2015) Visualizing translocation dynamics and nascent transcript errors in paused RNA polymerases in vivo. *Genome Biol* 16(1):98.

25. Larson MH*, et al.* (2014) A pause sequence enriched at translation start sites drives transcription dynamics in vivo. *Science* 344(6187):1042-1047.